SUPPLEMENTAL INFORMATION

Destruction and reconstruction of UO$_2^{2+}$ using gas-phase reactions

Michael J. Van Stipdonk[1*], Evan Perez[1†], Luke J. Metzler[1], Amanda R. Bubas[1‡], Theodore Corcovilos[2] and Arpad Somogyi[3]

[1]Department of Chemistry and Biochemistry, Duquesne University, Pittsburgh PA, USA
[2]Department of Physics, Duquesne University, Pittsburgh PA, USA
[3]Campus Chemical Instrument Center, The Ohio State University, Columbus OH, USA

Table S1. Product ion m/z values and compositions to accompany Figures 1 and 2 in the main text.

Table S2. Comparison of accurate m/z measurements, theoretical monoisotopic values, and molecule formulae for relevant ions in MS^n CID experiments initiated with [UO$_2$(O$_2$C-C$_6$F$_2$H$_3$)(CH$_3$CH$_2$OH)$_2$]$^+$ (Figure 1 of the main text).

Figure S1. Product in spectra generated by isolation of [UF$_2$(C$_2$H)]$^+$ for reaction with H$_2$O: (a) 1 ms isolation time, (b) 10 ms isolation time and (c) 100 ms isolation time. Figure 1d shows the product ion spectrum generated by dissociation of the ion-molecule reaction product at m/z 293.

Figure S2. Product ion spectra generated by isolation of [UF$_2$(OCH$_3$)]$^+$ for reaction with CH$_3$OH: (a) 1 ms, (b) 10 ms and (c) 100 ms.

Figure S3. Product ion spectra generated by CID of [UF(OCH$_3$)$_2$(CH$_3$OH)]$^+$ at m/z 351: (a) CID (MS^8 stage) of [UF(OCH$_3$)$_2$(CH$_3$OH)]$^+$, (b) CID (MS^9 stage) of [U(OCH$_3$)$_3$]$^+$ at m/z 331 and (c) CID (MS^{10}) of [UO(OCH$_3$)$_2$]$^+$ at m/z 316.

Figure S4. Product ion spectra generated by CID of species created by reaction of [UF$_2$(C$_2$H)]$^+$ with a mix of CH$_3$OH and CD$_3$OH: (a) isolation (MS^8 stage) of [UF$_2$(C$_2$H)]$^+$ for 100 ms for reaction with CH$_3$OH/CD$_3$OH, (b) CID (MS^9 stage) of [UF(OCH$_3$)$_2$]$^+$ at m/z 319, (c) CID (MS^9 stage) of [UF(OCH$_3$)(OCD$_3$)]$^+$ at m/z 322 and (d) CID (MS^9 stage) of [UF(OCD$_3$)$_2$]$^+$ at m/z 325. The spectrum shown in (e) shows the product ions generated by CID (MS^{10} stage) of [UOF(CD$_3$)]$^+$ at m/z 307.

Figure S5. Product ion spectra generated by CID of species created by reaction of [UF$_2$(C$_2$H)]$^+$ with CD$_3$OH: (a) CID (MS^8 stage) of [UF(OCD$_3$)$_2$(CD$_3$OH)]$^+$ at m/z 360, (b) CID (MS^9 stage) of [U(OCD$_3$)$_3$]$^+$ at m/z 340 and (c) CID (MS^{10} stage) of [UOF(OCD$_3$)$_2$]$^+$ at m/z 322.

Figure S6. Comparison of product ion spectra generated by isolation of species for reaction with H_2O. Figures S6(a)-S6(c) were generated by isolation of $[UO_2(F)]^+$ created by electrospray ionization of a solution of $[UO_2(F)_2]$. Figures S6(d)-S6(f) were created by isolation of the species at m/z 289 created by MS^n CID of $[UF(OCH_3)_2]^+$.

Figure S7. Comparison of product ion spectra generated by CID of species at m/z 301: (a) dissociation of $[UO_2(OCH_3)]^+$ created by solution of $UO_2(NO_3)_2$ in CH_3OH and (b) dissociation of ion at m/z 301 created by MS^n CID of $[UF(OCH_3)_2(CH_3OH)]^+$ that was generated by ion-molecule reactions of $[UF_2(C_2H)]^+$.

Scheme S1. Reaction pathways (dissociation and ion-molecule reaction) for species created by isolation and exposure of $[UF_2(C_2H)]^+$ to ca. 1 x 10^{-6} torr of CD_3OH directly admitted ion trap mass spectrometer.

Table S1.

MS^n CID of [UO$_2$(O$_2$C-C$_6$F$_2$H$_3$)(CH$_3$CH$_2$OH)$_2$]$^+$ (Figure 1)

m/z	Assigned composition
519	[UO$_2$(O$_2$C-C$_6$F$_2$H$_3$)(CH$_3$CH$_2$OH)$_2$]$^+$
491	[UO$_2$(O$_2$C-C$_6$F$_2$H$_3$)(CH$_3$CH$_2$OH)(H$_2$O)]$^+$
473	[UO$_2$(O$_2$C-C$_6$F$_2$H$_3$)(CH$_3$CH$_2$OH)]$^+$
445	[UO$_2$(O$_2$C-C$_6$F$_2$H$_3$)(H$_2$O)]$^+$
427	[UO$_2$(O$_2$C-C$_6$F$_2$H$_3$)(H$_2$O)]$^+$
401	[UO$_2$(C$_6$F$_2$H$_3$)(H$_2$O)]$^+$
383	[UO$_2$(C$_6$F$_2$H$_3$)]$^+$
381	[UO$_2$(C$_6$FO$_4$)]$^+$
355	[UO(C$_5$F$_2$H$_3$)]$^+$
329	[UO(C$_3$F$_2$H$_2$)]$^+$
327	[U(C$_4$F$_2$H$_3$)]$^+$
301	[UF$_2$(C$_2$H)]$^+$
293	[UF$_2$(OH)]$^+$
289	[UO$_2$(F)]$^+$
287	[UO$_2$(OH)]$^+$
276	[UF$_2$]$^+$
273	[OUF]$^+$

Reaction of [UF$_2$(C$_2$H)]$^+$ with CH$_3$OH (Figure 2)

m/z	Assigned composition
305	[UF(OH)(OCH$_3$)]$^+$
307	[UF$_2$(OCH$_3$)]$^+$
319	[UF(OCH$_3$)$_2$]$^+$
325	[U(C$_2$H)(OCH$_3$)$_2$]$^+$
331	[U(OCH$_3$)$_3$]$^+$
337	[UF(OH)(OCH$_3$)(CH$_3$OH)]$^+$
339	[UF$_2$(OCH$_3$)(CH$_3$OH)]$^+$
351	[UF(OCH$_3$)$_2$(CH$_3$OH)]$^+$
363	[U(OCH$_3$)$_3$(CH$_3$OH)]$^+$
369	[UF(OH)(OCH$_3$)(CH$_3$OH)$_2$]$^+$
371	[UF$_2$(OCH$_3$)(CH$_3$OH)$_2$]$^+$

CID of Ion-molecule Reaction Products (Figure 3)

304	[UOF(OCH$_3$)]$^+$
292	[UOF$_2$]$^+$

Table S2.

Measured m/z	Monoisotopic m/z	Error (ppm calc)	Formula	Composition Assignment
519.1344	519.1345	0.1926	$C_{11}H_{15}F_2O_6U$	$[UO_2(O_2C\text{-}C_6F_2H_3)(CH_3CH_2OH)_2]^+$
491.1022	491.1031	1.8326	$C_9H_{11}F_2O_6U$	$[UO_2(O_2C\text{-}C_6F_2H_3)(CH_3CH_2OH)(H_2O)]^+$
473.0919	473.0925	1.2683	$C_9H_9F_2O_5U$	$[UO_2(O_2C\text{-}C_6F_2H_3)(CH_3CH_2OH)]^+$
463.0710	463.0718	1.7276	$C_7H_7F_2O_6U$	$[UO_2(O_2C\text{-}C_6F_2H_3)(H_2O)_2]^+$
445.0605	445.0613	1.7750	$C_7H_5F_2O_5U$	$[UO_2(O_2C\text{-}C_6F_2H_3)(H_2O)]^+$
427.0500	427.0507	1.6392	$C_7H_3F_2O_4U$	$[UO_2(O_2C\text{-}C_6F_2H_3)]^+$
401.0708	401.0715	1.6456	$C_6H_5F_2O_3U$	$[UO_2(C_6F_2H_3)(H_2O)]^+$
399.0752	399.0757	1.2529	$C_6H_6FO_4U$	$[UO_2(C_6FOH_4)(H_2O)]^+$
383.0602	383.0608	1.5663	$C_6H_3F_2O_2U$	$[UO_2(C_6F_2H_3)]^+$
381.0647	381.0652	1.3121	$C_6H_4FO_3U$	$[UO_2(C_6FOH_4)]^+$
355.0655	355.0659	1.1266	$C_5H_3F_2OU$	$[UO(C_5H_3F_2)]^+$
353.0699	353.0703	1.1329	$C_5H_4FO_2U$	$[UO(C_5H_4OF)]^+$
329.0498	329.0503	1.4891	C_3HF_2OU	$[UO(C_3H_2F_2)]^+$
327.0706	327.0711	1.4370	$C_4H_3F_2U$	$[U(C_4H_3F_2)]^+$
301.0550	301.0554	1.4947	C_2HF_2U	$[UF_2(C_2H)]^+$
293.0499	293.0503	1.3650	HF_2OU	$[UF_2(OH)]^+$
292.0420	292.0425	1.7121	F_2OU	$[UF_2(O)]^+$
289.0385	289.0390	1.7299	FO_2U	$[UO_2(F)]^+$
287.0430	287.0434	1.2890	HO_3U	$[UO_2(OH)]^+$
276.0472	276.0476	1.4490	F_2U	$[UF_2]^+$
273.0437	273.0441	1.4650	FOU	$[OUF]^+$
270.0402	270.0406	1.3331	O_2U	$[UO_2]^+$

Figure S1.

(a)

519
473
427
383
355
301 307

307
$[UF_2(OCH_3)]^+$

319
325

(b)

307

$[UF(OCH_3)_2]^+$
319

$[UF_2(OCH_3)(H_2O)]^+$
325
351

(c)

351
$[UF(OCH_3)_2(CH_3OH)]^+$

319
$[UF(OCH_3)_2]^+$

305,
307

337,
339

369,
371

250   275   300   325   350   375
m/z

Figure S2.

6

Figure S3.

Figure S4.

(a)
- 519
- 473
- 427
- 383
- 355
- 301 → 360

325
[UF(OCD₃)₂]⁺

-35
(CD₃OH)

-20
(HF)

[U(OCD₃)₃]⁺
340   **360**

(b)
- 519
- 473
- 427
- 383
- 355
- 301 → 360
- 340

322
[UOF(OCD₃)₂]⁺

-18
(CH₃)

[U(OCD₃)₃]⁺
340

304

(c)
- 519
- 473
- 427
- 383
- 355
- 301 → 360
- 340
- 322

304
[UO₂(OCD₃)]⁺

-18
(CH₃)

[UOF(OCD₃)₂]⁺
322

250   275   300   325   350   375
m/z
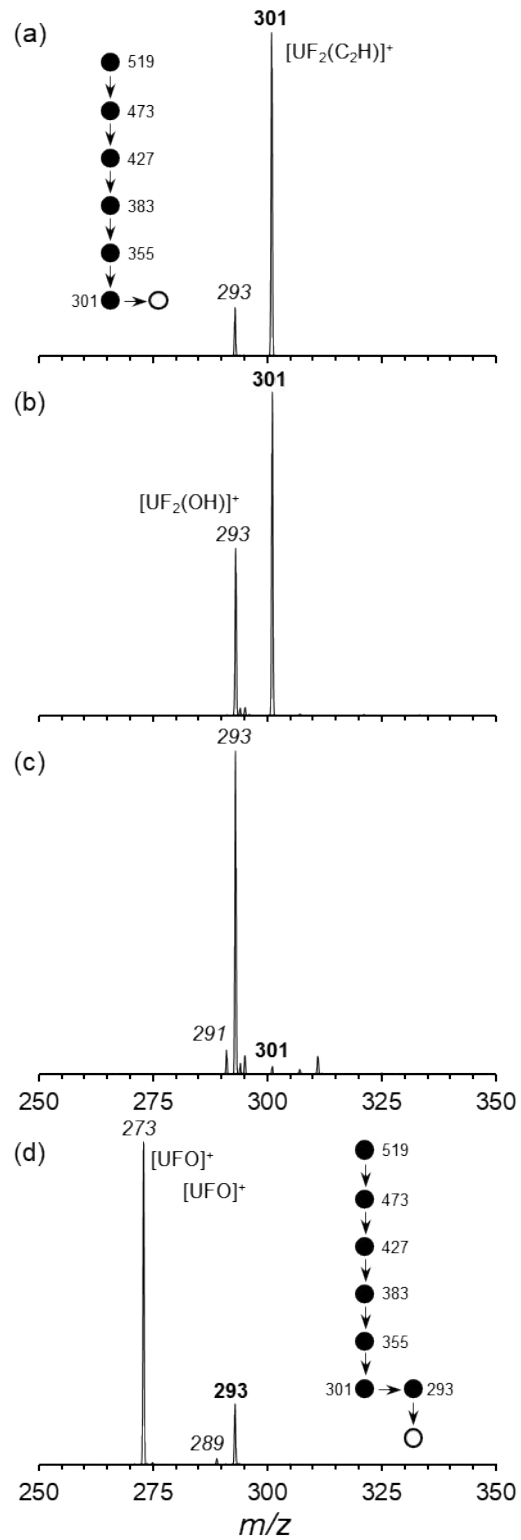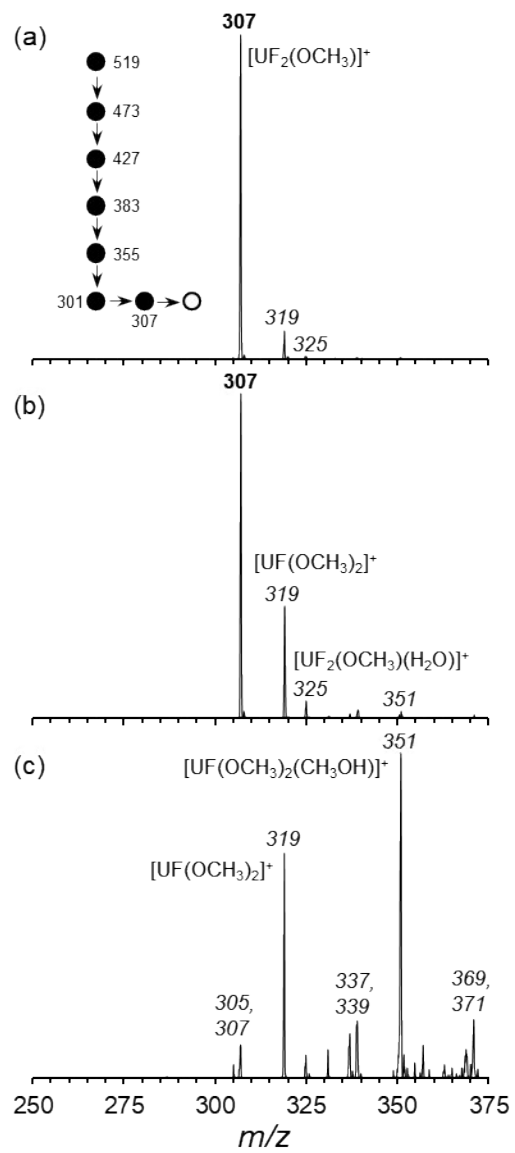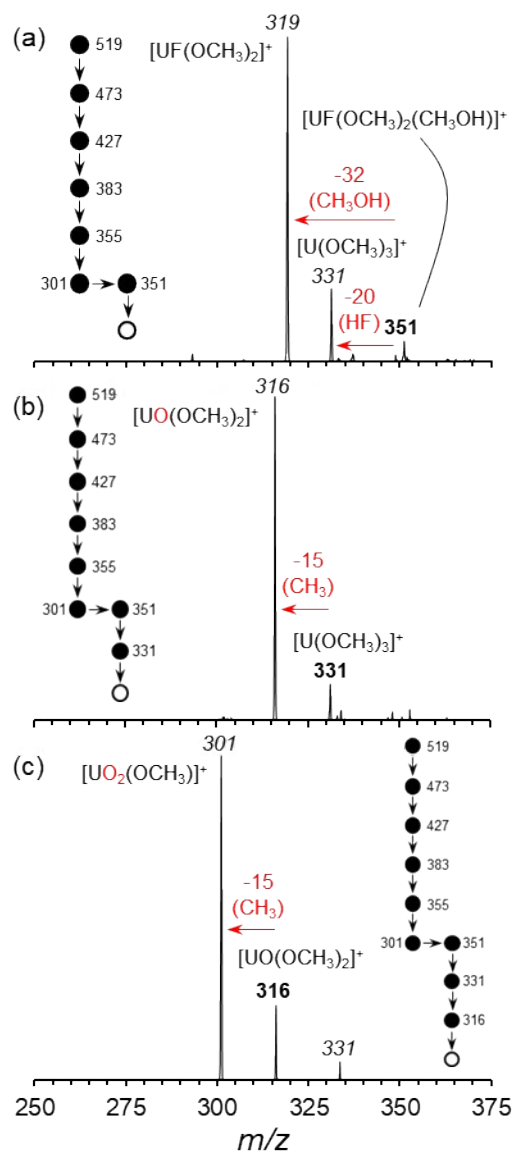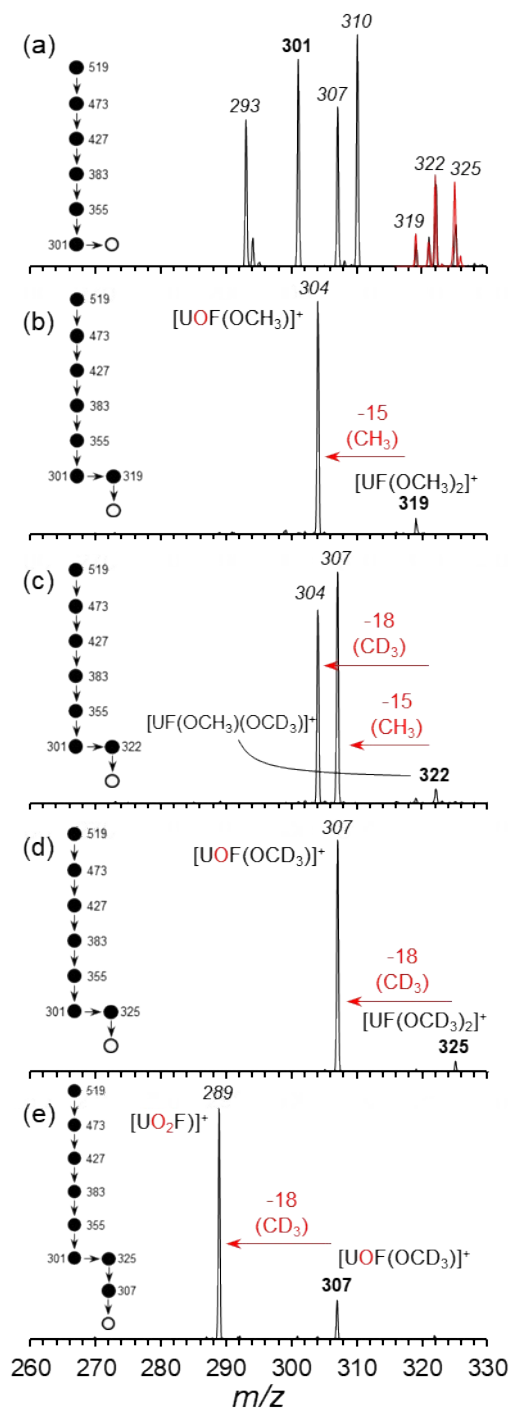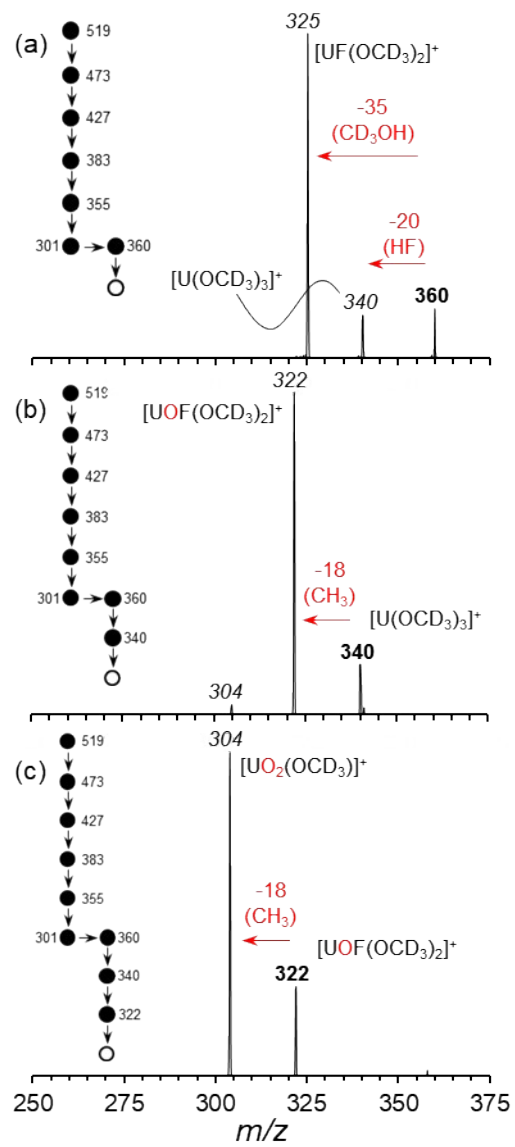
Figure S5.

Isolation of [UO$_2$(F)]$^+$ (m/z 289) derived from solution of UO$_2$(F)$_2$ in H$_2$O/CH$_3$OH

Isolation of m/z 289 after creation by ion-molecule reactions and CID in this study

(a)   **289**

287

(b)   **289**

287

(c)   287

289

250   275   300   325
m/z

(d)   **289**

[UO$_2$(F)]$^+$

[UO$_2$(OH)]$^+$

287

(e)   **289**

287

(f)   287

289

250   275   300   325
m/z
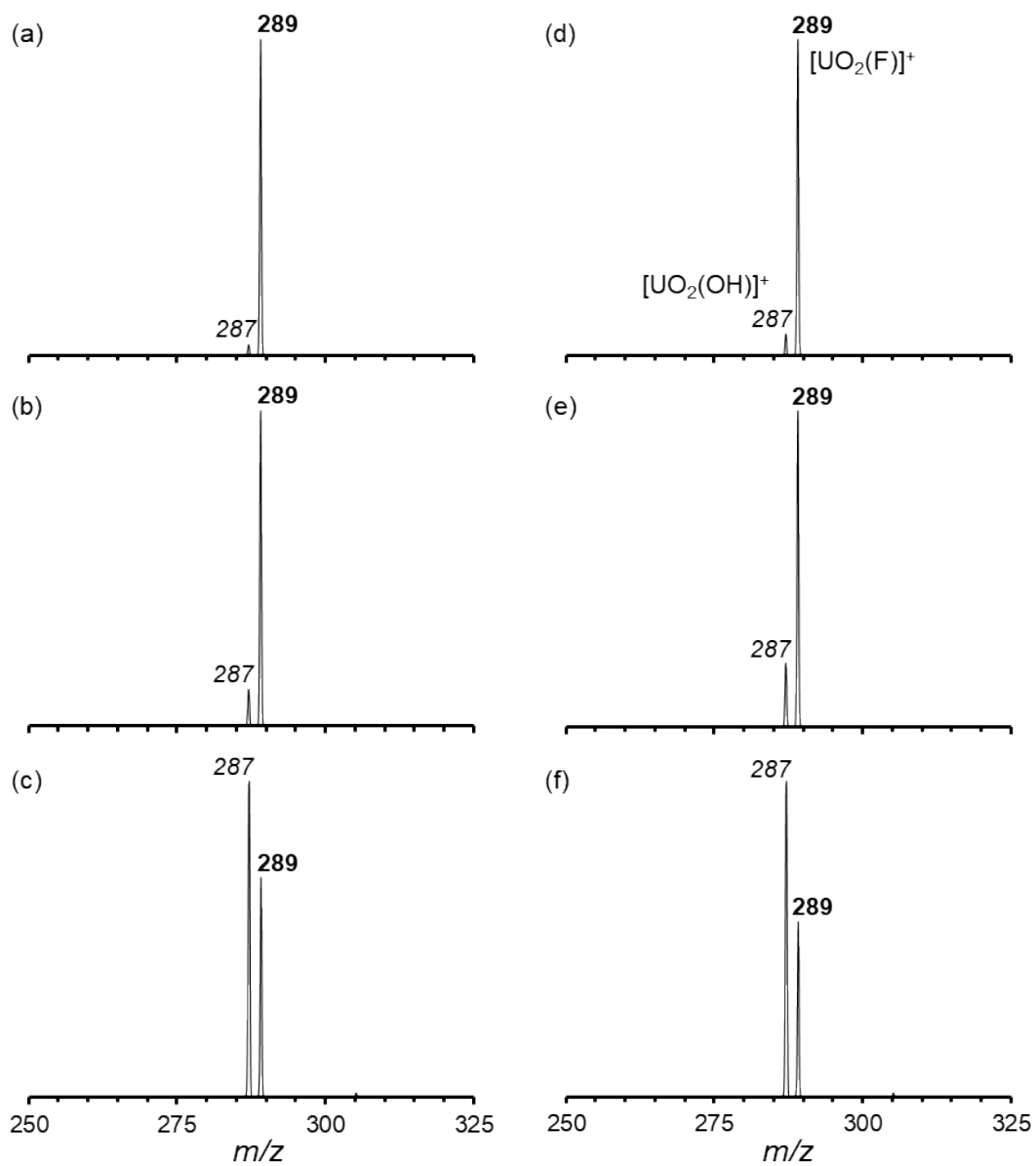
Figure S6.

Figure S7.

Scheme S1.

301 [UF$_2$(C$_2$H)]$^+$

$\xrightarrow{\text{+9 (+CD}_3\text{OH, -C}_2\text{H}_2\text{)}}$ 310 [UF$_2$(OCD$_3$)]$^+$

$\xrightarrow{\text{+15 (+CD}_3\text{OH, -HF)}}$ 325 [UF(OCD$_3$)$_2$]$^+$

$\xrightarrow{\text{+35 (+CD}_3\text{OH)}}$ 360 [UF(OCD$_3$)$_2$(CD$_3$OH)]$^+$

−18 (−CD$_3$) → 292 [UOF$_2$]$^+$

−18 (−CD$_3$) → 307 [UOF(OCD$_3$)]$^+$

−18 (−CD$_3$) → 325 [UOF(OCD$_3$)$_2$]$^+$

−35 (−CD$_3$OH) → 325 [UOF(OCD$_3$)$_2$]$^+$

−20 (−HF) → 340 [U(OCD$_3$)$_3$]$^+$

Ion-molecule reaction
Collision-induced dissociation

−18 (−CD$_3$) → 289 [UO$_2$F]$^+$

−18 (−CD$_3$) → 322 [UO(OCD$_3$)$_2$]$^+$
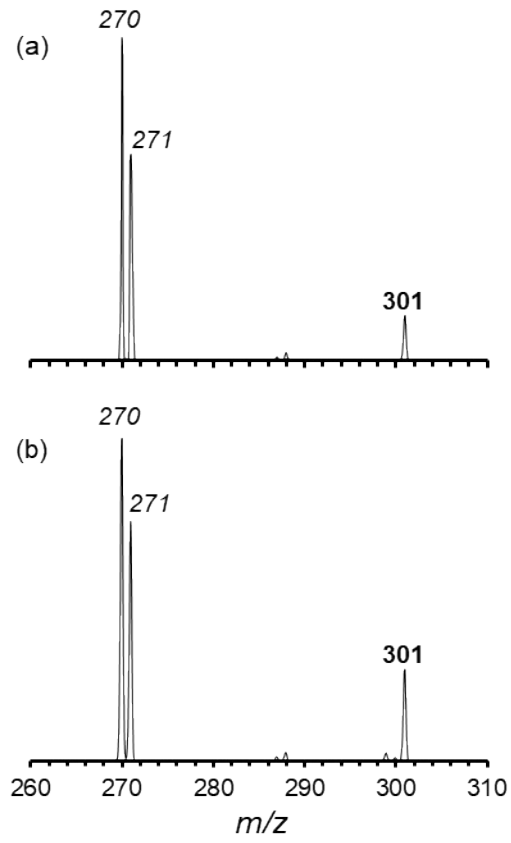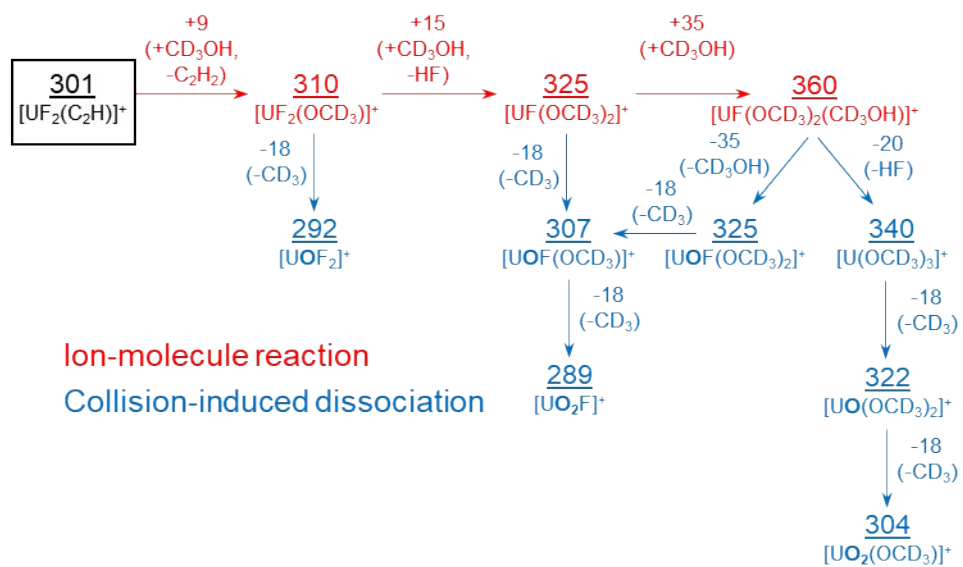
−18 (−CD$_3$) → 304 [UO$_2$(OCD$_3$)]$^+$

12

EXPERIMENTAL METHODS

Sample Preparation

Methanol (CH_3OH), labeled methanol (CD_3OH), ethanol (CH_3CH_2OH) and 2,6-difluorobenzoic acid were purchased from Millipore-Sigma (St. Louis, MO) and used as received.   The sample used to prepare gas-phase $[UO_2(O_2C-C_6F_2H_3)]^+$ was created by combining 2-3 mg of $U^{VI}O_3$ (Strem Chemicals, Newburyport MA), corresponding to approximately 7×10^{-6} to 1×10^{-5} moles, with a 2-fold mole excess of propiolic acid (Sigma Aldrich, St. Louis MO) and 400 ◦L of deionized/distilled H_2O in a glass scintillation vial. The solutions were incubated on a hot plate at 70°C for 12 hours. *Caution: uranium oxide is radioactive (α- and γ-emitter), and proper shielding, waste disposal and personal protective gear should be used when handling the material.* When cooled, 20 µL of the resulting solution was diluted with 800 µL of 90:10 (by volume) $H_2O:CH_3CH_2OH$ and used without further work up as the spray solution for electrospray ionization (ESI).

ESI and CID experiments were performed on a ThermoScientific (San Jose, CA) LTQ-XL linear ion trap (LIT) mass spectrometer. Solutions for ESI were infused into the instrument using the incorporated syringe pump at a flow rate of 5 µL/min. In the positive ion mode, the auto-tune routine within the LTQ Tune program was used to optimize the atmospheric pressure ionization stack settings for the instrument (lens voltages, quadrupole and octopole voltage offsets, etc.) to achieve maximum transmission of singly charged ions such as $[UO_2(O_2C-C_6F_2H_3)(CH_3CH_2OH)_2]^+$ to the LIT. Helium was used as the bath/buffer gas to improve trapping efficiency and as the collision gas for CID experiments.

For multiple-stage (MS^n) CID experiments to probe fragmentation and ion-molecule reaction (IMR) pathways, precursor ions were isolated using a width of 1.0 to 1.5 mass to charge (*m/z*) units. The exact value was determined empirically to provide maximum ion intensity while ensuring isolation of a single isotopic peak. To probe CID behavior, the (mass) normalized collision energy (NCE, as defined by ThermoScientific) was set between 5 and 18%, which corresponds to 0.075 - 0.27 V applied for CID with the current instrument calibration. The activation Q, which defines the frequency of the applied radio frequency potential, was set at 0.30 and a 30 ms activation time was used.

We have installed a gas manifold on the buffer gas inlet of our instrument to allow the mixing of reagents with the helium buffer gas before introduction into the ion trap. Liquid reagents are introduced into the manifold from a metered syringe pump, where they evaporate. The partial pressure of these reagents may be controlled through the syringe pump rate, the helium flow rate, and by heating or cooling the manifold, which is done by wrapping the manifold tubing with a temperature-controlled water coil. All gas ports are controlled by manually actuated precision needle valves, which provide control of the flow rates. The helium buffer gas flow rate is monitored with an electronic mass flow meter and flow is controlled by the needle valve to the exhaust line. When operating the mass spectrometer without additional

reagents, three-way valves route the buffer gas through a clean section of tubing. The reagent pathway may be purged by flushing with clean gas (e.g., nitrogen) into a vacuum pump. The vacuum pump is preceded by a cold trap to aid in the removal of volatile reagents. The entire manifold is constructed from stainless steel tubing and components using stainless steel compression fittings, so that it may be periodically removed and baked in an oven for cleaning.

To probe gas-phase reactions of selected precursor ions with background neutrals, ions were isolated using widths of 1-2 m/z units. Here too, the specific width used was chosen empirically to ensure maximum ion isolation efficiency. The ions were then stored in the LIT for periods ranging from 1 ms to 10 s. When examining ion-molecule reactions (IMRs), our intent was not to measure or report rates or rate constants, but to identify the *pathways* by which ions react with neutrals such as H_2O or CH_3OH in the LIT. Because the experiments were performed using the multi-dimensional tandem mass spectrometry capabilities of the linear ion trap, care had to be taken to ensure that enough neutral reagent was present in the ion trap for ion-molecule reaction studies, without hampering the "synthesis" of the [OUCH]+ precursor ion by repeated CID steps. For both CID and IMR experiments, the mass spectra displayed were created by accumulating and averaging at least 30 isolation, dissociation, and ejection/detection steps.

High-resolution/high-accuracy measurements were performed on a ThermoScientific (San Jose, CA) LTQ-Orbitrap Elite mass spectrometer using experimental conditions and settings like those outlined above for the LTQ-XL instrument. With the Orbitrap instrument, the experiments were performed with the 120,000 resolution setting, NCE values of 8 – 16%, activation Q setting of 0.25, and a 10 ms activation time. Mass spectra were collected for 1 minute at each MS[n] stage.